On Equatorial Waves and El Niño. I: Influence of Initial States on Wave-Induced Currents and Warming

PAUL S. SCHOPF

Goddard Laboratory for Atmospheric Sciences, NASA/Goddard Space Flight Center, Greenbelt, MD 20771

D. E. HARRISON

Department of Meteorology and Physical Oceanography, Massachusetts Institute of Technology, Cambridge, MA 02139

(Manuscript received 21 October 1982, in final form 18 March 1983)

ABSTRACT

We present results from three numerical model experiments designed to study the thermal and hydrodynamical changes associated with downwelling Kelvin wave passage and east coastal reflection along and near the equator. The model employs primitive equation dynamics in two active layers and a full thermodynamics equation, so that sea surface temperature, thermocline displacement and sea level are each independently predicted. Wind and thermal forcing are used. The surface layer is a slab mixed layer using Kraus and Turner-style bulk physics. Kelvin waves are excited by introducing a westerly wind anomaly in the western part of the basin, and the temperature and current changes caused by the waves are studied as the wave fronts propagate through the circulation forced by three different mean wind fields: no mean winds, southerly mean winds and easterly mean winds. The wave-induced changes depend strongly on the conditions that prevail when the waves are forced. Anomalous advection of the existing SST field is the primary SST change mechanism. The two internal Kelvin–wave modes allowed by the model sometimes induce comparable temperature changes near the east coast and sometimes the effect of one mode substantially dominates that of the other. The shear mode wave does not always propagate to the east coast; it can be destroyed by nonlinear effects associated with the meridional circulation along the equator. Temperature changes near the east coast, similar in magnitude to those observed in the early stages of El Niño events, are caused in the mean southerly wind case, but no broad westward tongue appears later on. The implications of these results on existing models of El Niño and for future model studies are examined.

1. Introduction

The equatorial wave guide supports the existence of fast, zonally propagating linear waves whose dynamics have long been known, e.g., Matsuno (1966) and Moore and Philander (1976). Simple forced systems have also been explored, e.g., Cane and Sarachik (1976, 1977). Of the large-scale, low frequency free waves, the fastest are the eastward-propagating equatorial Kelvin waves; the fastest westward-propagating waves are the equatorially trapped Rossby waves travelling at ⅓ the Kelvin-wave speed. These waves are easily forced by abrupt changes in wind stress along the equator, and it has been suggested that they play a fundamental role in the interannual variations of the tropical Pacific known as El Niño (e.g., Hurlburt *et al.*, 1976; McCreary, 1976; Busalacchi and O'Brien, 1981; Philander, 1981).

Rasmusson and Carpenter (1982) have described the character of a composite El Niño event developed from surface ship reports. Based on sequential three-month average fields of temperature, wind and wind divergence, they suggest that there are atmospheric anomalies in the western Pacific sometime in the late fall and early winter preceeding an El Niño event and that there is simultaneously some weak equatorial warming near the Dateline. In the late winter, SST along the coast of South America south of the equator begins to rise more rapidly than during a normal annual cycle until the temperature is a few degrees warmer than climatology. Anomalously warm water then begins to be evident further off the South American coast, as shown in their analysis of the "peak phase" presented here in Fig. 1. Later evolution into the transition and mature phases shows substantial broad warming along the equator with 1°C anomalies out to the Dateline. We are interested here in the onset and early stages—the first appearance of warm water at the eastern end of the equator, with an anomalous temperature of approximately 2°C.

Clearly it would be of great interest to understand how this dramatic event takes place. Most previous model studies have highly idealized the relationship between hydrodynamic and thermodynamic quantities (although cf. Philander, 1981 and references therein). For example, single-layer reduced gravity models assume that SST changes are directly related to pycnocline depth changes, the dynamic quantity

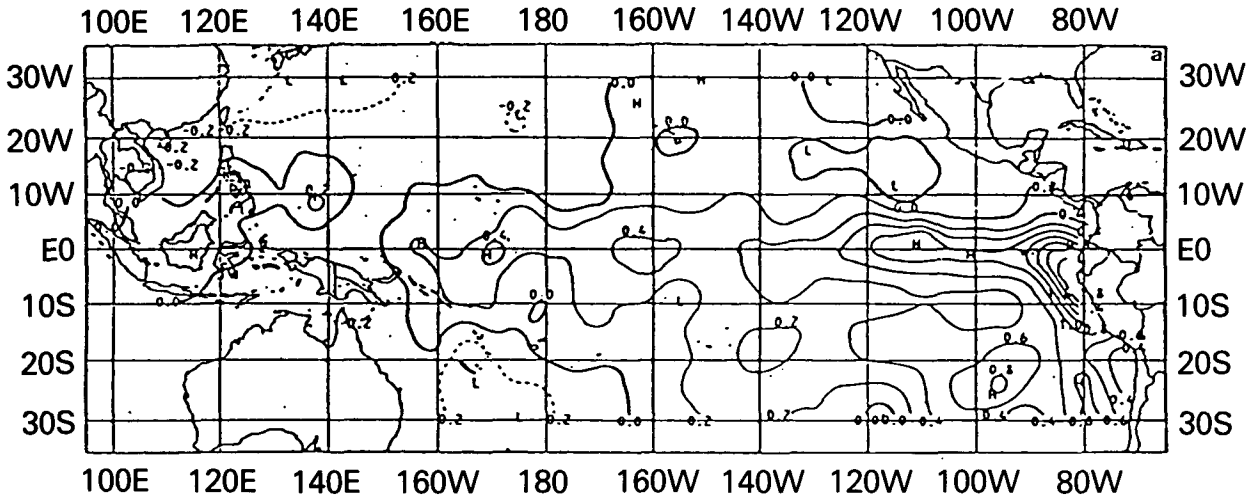

FIG. 1. SST anomaly from Rasmusson and Carpenter (1982) for the peak phase of El Niño. Contour interval = 0.6°C.

computed in these models. Sea level changes are also directly related to pycnocline depth changes, and are not an independent physical quantity in these systems. These convenient simplifications deserve further investigation since it is SST, not sea level or thermocline depth, that is of primary climatic interest. It is clear that the hydrodynamic conditions can change importantly over very short timescales, but the thermodynamic changes have not been thoroughly studied.

The mean flow in the tropical upper ocean is generally believed to be non-linear, with strongly coupled thermo- and hydrodynamic processes (although cf. McCreary 1981 for a linear model of equatorial circulation that reproduces a number of observed features). Whether the linear wave ideas and simple model results continue to apply to perturbations of non-linear and thermally coupled flows remains to be seen.

Rather than attempt to simulate the El Niño phenomena, we will investigate the specific thermal and hydrodynamic changes induced by a single candidate mechanism for the onset of El Niño: the remotely forced Kelvin-wave front. We present experiments with a non-linear model that includes hydro- and thermodynamics. It is an extension of the model of Schopf and Cane (1983), which has been shown to simulate many fundamental features of the tropical circulation. Three experiments are reported as our first investigation into the interaction between equatorial waves and thermo- and hydrodynamic changes in the equatorial ocean. The first experiment is run with no mean wind forcing, and is included for comparison with previous linear studies. A second case is run with mean southerly winds, to illuminate aspects of the wave-induced changes in the cold water pool adjacent to the eastern coast that is forced by wind-driven upwelling. A case with mean easterly winds introduces the effects of temperature gradients along the equator as well as an equatorial undercurrent and sloping main thermocline. We shall show that the effects of the waves in this model system are strongly dependent upon the mean state that exists before the wind anomaly initiates the wave front.

2. Model description

The model used is that of Schopf and Cane (1983), modified to facilitate long term computations in a more efficient manner. Two layers are used above a quiescent abyssal ocean, with primitive equations used to predict velocities in each layer. The top layer is the wind-mixed layer, its depth predicted by bulk energy balances as introduced by Kraus and Turner (1967). Continuity for the two layers gives

$$\partial(h_1)/\partial t + \nabla\cdot(h_1\mathbf{V}_1) = w_e, \tag{1}$$

$$\partial(h_2)/\partial t + \nabla\cdot(h_2\mathbf{V}_2) = -w_e. \tag{2}$$

Conservation of heat for the two layers requires

$$\partial(h_1T_1)/\partial t + \nabla\cdot(h_1\mathbf{V}_1T_1) = Q + w_e[H(w_e)T_e + H(-w_e)T_1], \tag{3}$$

$$\partial(h_2T_2)/\partial t + \nabla\cdot(h_2\mathbf{V}_2T_2) = -w_e[H(w_e)T_e + H(-w_e)T_1]. \tag{4}$$

The nonlinear primitive equation momentum balance is

$$\partial(h_1\mathbf{V}_1)/\partial t + \nabla\cdot(h_1\mathbf{V}_1\mathbf{V}_1) + f\mathbf{k}\times h_1\mathbf{V}_1 = \tau - h_1[\nabla(b_1h_1 + b_2h_2) - h_1\nabla b_1/2] + w_e[H(w_e)\mathbf{V}_2 + H(-w_e)\mathbf{V}_1], \tag{5}$$

$$\partial(h_2\mathbf{V}_2)/\partial t + \nabla\cdot(h_2\mathbf{V}_2\mathbf{V}_2) + f\mathbf{k}\times h_2\mathbf{V}_2$$
$$= -h_2[\nabla(b_2h_2/2) + b_2\nabla(h_1 + h_2/2) - \Gamma_b\nabla h_2/6$$
$$- \nabla\Gamma_b h_2/12] - w_e[H(w_e)\mathbf{V}_2 + H(-w_e)\mathbf{V}_1], \quad (6)$$

where h_k, $\mathbf{V}_k$, T_k are the depth, mean velocity and mean temperature of the kth layer. Here τ and Q are the surface fluxes of momentum and heat, and b_k is the buoyancy, given by

$$b_k = g\alpha(T_k - T_r), \quad (7)$$

where T_r is the reference temperature of the abyssal ocean. In (6) Γ_b is the effective buoyancy gradient in the second layer; it is defined differently in the present model than in Schopf and Cane (1983) as will be described below. In (1)–(6) w_e is the entrainment rate across the base of the mixed layer, and H is the Heaviside step function.

In Schopf and Cane, the temperature at the base of the second layer (T_b) is allowed to warm up if a linearly extrapolated temperature profile gives rise to static instability at the base of the mixed layer. Thus, T_b can be raised but cannot be lowered. For short runs (a few months) this has posed little problem, but we have been unable to reach satisfactory equilibrium states in multi-year runs with the previous model. In order to avoid this difficulty, we choose to fix T_b, returning to the view that the base of the second layer is a material surface. Thus Schopf and Cane's Eq. (2.17) becomes

$$T_b = 14.5°\text{C}. \quad (8)$$

It remains to specify a thermal profile in the second layer based on T_2 and T_b, which are our only degrees of freedom, that will give a good approximation to the temperature at the base of the mixed layer. This choice will affect both the entrainment and the pressure term for the second layer.

We begin by seeking a linear temperature profile, and we extrapolate from T_b and T_2 to obtain a provisional temperature just below the mixed layer:

$$T_e^* = 2T_2 - T_b. \quad (9)$$

If $T_e^* \leqslant T_1$, the profile is stable and the linear profile is our solution ($T_e = T_e^*$). The initial conditions are set up with $T_e^* \leqslant T_1$ and this is generally maintained.

However, detrainment leaves behind a more complex thermal profile, with water at the surface temperature left in the top of the second layer. This increases the mean temperature of the second layer and can give an extrapolated T_e^* warmer than T_1. In this case we reject the linear profile in favor of a second layer profile that has a certain thickness of water at temperature T_1 overlying a linearly stratified region, as shown in Fig. 2 ($T_e = T_1$). The new profile must have a heat content equal to T_2h_2. This sets the depth of the auxillary layer (h_A):

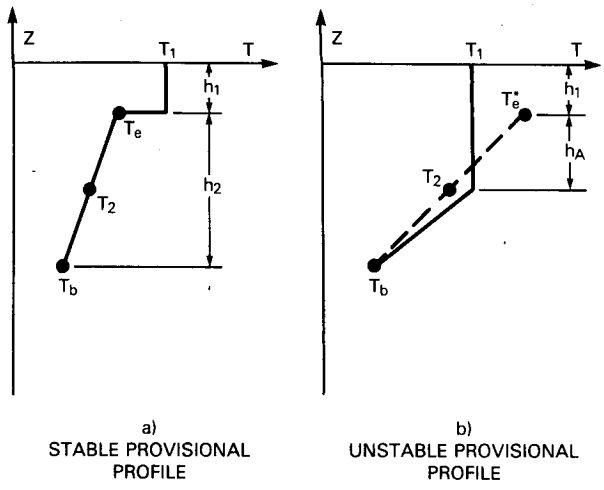

FIG. 2. Vertical structure of the model temperature field. When the extrapolated temperature at the base of the mixed layer is less than the surface temperature, profile (a) is used; otherwise, there is an isothermal region at the top of the second layer at T_1 as in (b). The thickness of this layer is given by (10).

$$h_A = h_2(T_e^* - T_1)/(T_1 - T_b), \quad (10)$$

where T_e^* is the provisional (unstable) extrapolated temperature from (9). When this auxillary layer is present, the pressure term must reflect the change in density structure. The integrated pressure gradient (P_2) is obtained by integrating ($\nabla p + b\nabla z$) through the second layer:

$$P_2 = h_2[\nabla(b_2h_2/2) + b_2\nabla(h_1 + h_2/2)]$$
$$- \nabla h_2^2[(b_e^* - b_b) - 2(b_e^* - b_1)^2/(b_1 - b_b)], \quad (11)$$

where b_e^* and b_b are the buoyancies associated with T_e^* and T_b. Eq. (2.14) of Schopf and Cane (1983) remains valid if we re-interpret Γ_b as:

$$\Gamma_b = b_e^* - b_b - H(h_A)2\frac{(b_e^* - b_1)^2}{(b_1 - b_b)}. \quad (12)$$

The second part on the right hand side only enters if h_A is positive; $h_A = 0$ gives Γ_b the same as in Schopf and Cane.

As in Schopf and Cane (1983), the entrainment is evaluated by an analytic integration of Niiler and Kraus' (1977) entrainment equation:

$$w_eH(w_e)\{h_1(b_1 - b_e)\}$$
$$= 2m_su_*^3 - 2\epsilon_0h_1 + h_1g\alpha Q. \quad (13)$$

This is a specification of the bulk energy balance mixed layer model, which retains wind stirring, surface heating, dissipation and the potential energy change associated with deepening. The turbulence level changes, shear production at the base of the mixed layer and the depth-dependent component of penetrating radiation are dropped. When $w_e < 0$ (13)

is used to solve for the new h, and (1) is used to elevate w_e. As in Schopf and Cane, a minimum layer thickness is used to maintain numerical stability and to model the otherwise unspecified effects of wave breaking, near-surface absorption of penetrating radiation, and near-surface shear production.

The other model modification was the introduction of grid stretching in the zonal direction, with a resolution of 25 km at the eastern wall and 200 km in the interior of the basin.

For the cases reported here, we have specified the surface heat flux as proposed by Haney (1971):

$$Q = K(T_a - T_1), \tag{14}$$

with $T_a = 29.0°C$ and $K = 30$ W m^{-2} K^{-1}. The mixed layer equations are solved with $u_* = 0.864$ cm s^{-1}, $m_s = 1.25$, $\epsilon_0 = 7.5 \times 10^{-9}$ and $g\alpha = 2. \times 10^{-3}$. The initial temperature profile was taken with $T_1 = 28.°C$, $T_2 = 19.5°C$, $T_b = 14.5°C$, $T_r = 10.5°C$, $h_1 = 50$ m, $h_2 = 150$ m. The basin extends over 75° of longitude, and 40° of latitude. The walls are treated as rigid, with no-slip boundary conditions.

3. Results

In this section we examine the equatorial response to waves forced by turning on a westerly anomaly in the western part of the basin. The stress anomaly extends from 10° to 37.5° longitude and from the southern to northern basin boundaries. It is turned to full strength linearly in time over 5 days, has an amplitude of 0.5 dyn cm^{-2} within the patch, and tapers to 0.0 over 5 degrees inside the boundaries of the patch. Once turned on, the anomaly remains on. Three different mean environments are examined: no wind, uniform southerly wind, and uniform easterly wind.

The model allows two internal modes of motion. Based upon the initial stratification, their linear phase speeds are 1.88 and 0.63 m s^{-1}. It thus takes 25.6 days for the gravest mode Kelvin wave (K_1) to propagate from the eastern end of the forcing region to the eastern end of the basin at 75° longitude. The other, shear mode Kelvin wave (K_2) takes 76.5 days.

a. No mean wind

This case is most similar to previous Kelvin wave studies, as the background initial state has spatially uniform thermodynamic quantities and no mean circulation. Fig. 3 shows the response along the equator east of the wind anomaly, with $t = 0$ as the anomaly is turned on and continuing for 180 days. Time-longitude plots of SST (T_1), pycnocline depth ($h_1 + h_2$), surface height ($[b_1h_1 + b_2h_2]g^{-1}$), and zonal velocity vertical shear ($u_1 - u_2$) are shown; they reveal the relevant details of the response for this discussion.

From Fig. 3a it is clear that there is no perceptible

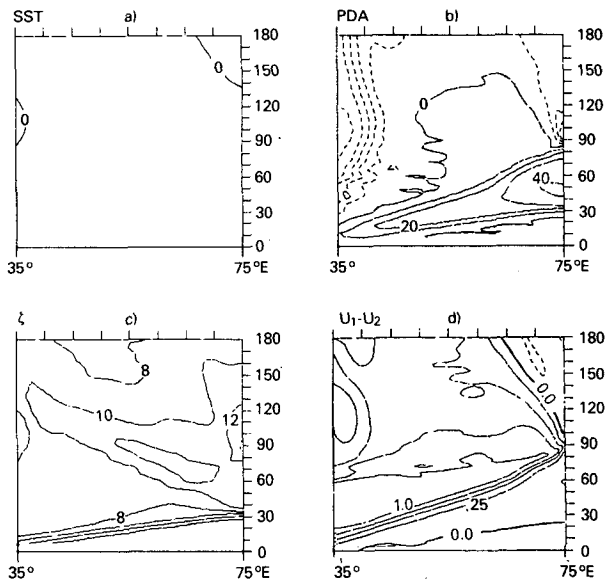

FIG. 3. Equatorial time–longitude sections of the model results with no mean winds. A westerly wind perturbation is imposed from 10 to 37.5°E from day 0 and held constant. a) SST, contour interval 0.5°C, b) pycnocline depth anomaly, contour interval 10 m, positive downwards, c) surface dynamic height, contour interval 2 cm, positive upwards, d) zonal velocity shear between mixed layer and stratified layer, contour interval 0.25 m s^{-1}.

change in SST as the two Kelvin waves (K_1 and K_2) propagate in from the wind patch. Over the full 180-day period, the maximum SST change is less than 1°C, so neither the Kelvin nor the Rossby waves change SST in this situation. The eastward propagation of K_1 is seen most clearly in the surface height (Fig. 3c), and this wave front reaches the eastern boundary in ~27 days which is very close to the linear prediction of 26 days. This wave accelerates the flow eastward in both dynamic layers and drives both layers downward, so K_1 can also be followed in pycnocline depth (Fig. 3b). In this case K_2 is a shear mode which accelerates the surface layer eastward and layer 2 westward; it increases h_1 but decreases h_2 more and thereby compresses and raises the thermocline. Here K_2 is best followed in $u_1 - u_2$ (Fig. 3d), but can also be seen in pycnocline depth; it is not evident in surface height. Kelvin wave K_2 reaches the coast in about 80 days, which also agrees well with linear prediction.

In Fig. 4, we present longitude–depth sections of the equatorial temperature field east of the wind anomaly, at 20 day intervals. At $t = 20$ days, the leading edge of the K_1 front is near 65° longitude and the leading edge of the K_2 front is near 47°; K_1 is driving down the pycnocline, and depressing the isotherms throughout the second layer, and K_2 is pinching the isotherms in the second layer. By day 40, K_1 has reflected off the coast, and the predicted location of the leading edge of the first mode Rossby wave

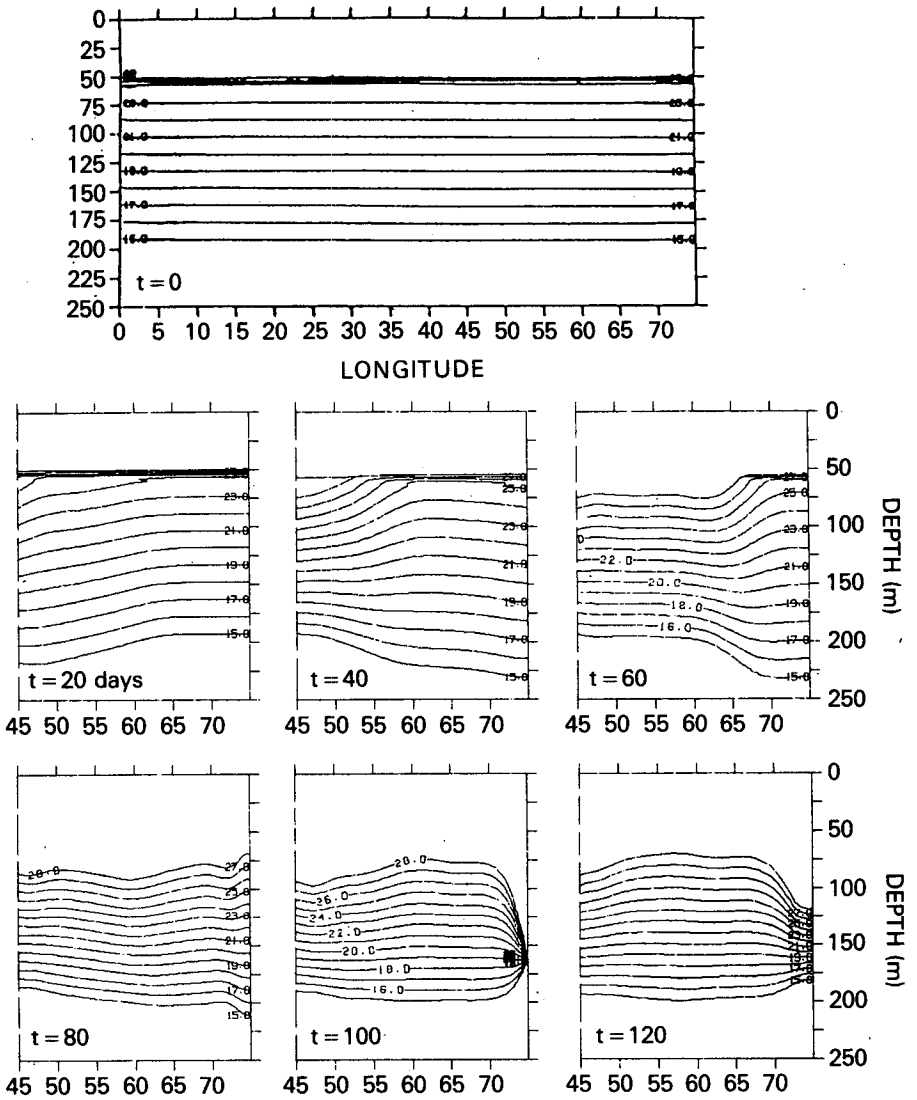

FIG. 4. Equatorial temperature sections from the case with no mean winds. Panels are separated by 20 day intervals, and only the eastern, unforced region is shown. Contour interval 1°C. Within the second layer, the linear temperature profile from Fig. 2 is used to plot the thermal field.

(R_1) is 68°; at the coast the 15°C isotherm has deepened from 200 to 230 m and the temperature at 75 m has warmed from 23.0 to 24.5°C. The second mode Kelvin wave front (K_2) has now propagated to about 57° longitude, and its pinching influence is clear. Between 40 and 60 days, little changes at the eastern end of the equator; the 15° isotherm remains at 230 m, and the 75 m temperature stays ~24.5°C.

With the arrival of K_2, between 60 and 100 days, a dramatic change occurs in the coastal conditions; the 15°C isotherm is raised sharply, while all isotherms greater than 21°C are depressed. The 75 m temperature rises another 3.5°C, to 28.0. Subsequent reflection in R_2 spreads this near surface warming, although this occurs very slowly. (At day 100, h_2 is non-zero but there is a large isothermal portion within layer 2 giving no computational difficulties).

In this experiment we see the two Kelvin waves propagate in to the coast very clearly at speeds predicted by linear wave theory, but with no SST change. Upon reflection K_1 produces some coastal subsurface warming but still no SST change. The K_2 reflection gives substantial subsurface warming, yet no SST change. The outgoing Rossby waves also produce no significant SST change.

The reason for a lack of change in SST is the absence of any horizontal gradients in SST and the fact that the Kelvin waves that were excited produced downwelling. As discussed in Schopf and Cane (1983) a downwelling is likely to lead to detrainment or ex-

pulsion of water from the mixed layer. This process does not lead to warming of the surface water; it warms the sub-surface water.

b. *Mean southerly winds*

The thermal state of the surface layer is maintained through a balance of entrainment cooling, horizontal advection and surface heating. The introduction of a mean state with surface currents and upwelling permits wave frontal passage to affect this balance and so produce significant SST changes.

Uniform southerly winds of 0.5 dyn cm^2 provide the initial conditions for this experiment. Coastal upwelling, driven by surface Ekman current divergence, produces a cool pool of surface water (minimum SST = 23.9°C) along the eastern boundary south of the equator. Along the equator there is almost no change in temperature or layer thicknesses and these fields are nearly identical to those in the previous case. At the end of a 360 day spin-up period the cooling due to entrainment at the coast is balanced by heating from the atmosphere and advection. The initial conditions for the wind anomaly response now include SST gradients and currents.

Along the equator the response in SST, pycnocline height, surface elevation and current shear (Figs. 5, 6) are similar to those in the case with no mean winds. Again, K_1 arrives at the coast after about 28 days and causes little change. Also K_2 propagates with about the same speed, but is slowed somewhat as it reaches the coast, and so the coastal response is delayed by about 20 days.

The first significant changes in SST are found south of the equator along the coast and are brought about by the Kelvin waves. Fig. 7 gives latitude-time sections of change in SST from the spun-up value approximately 200 km offshore. After 40 days K_1 has reached the coast and continued down the coast to 20°S. The warming is seen to occur with the arrival of K_1 and is strengthened with the arrival of K_2; closer to the coast warming subsequent to K_2 arrival is stronger and ΔSST can be 4°C. The lack of any warming near the equator is due to the fact that the temperature of water there was greater than 28°C initially, and the model includes no processes that can warm it further.

Fig. 8 shows latitude–depth sections of temperature along the eastern wall for the Southern Hemisphere. At the onset of the perturbing winds, the coastal upwelling has produced a cold, shallow mixed layer at 10°S, but relatively warm temperatures along the equator. After 40 days, K_1 has arrived and has depressed the 15°C isotherm from 175 to 250 m. The first mode character of this response is evident (isotherms throughout the second layer are depressed, more at the bottom). At 5°S, the SST was 25°C, but

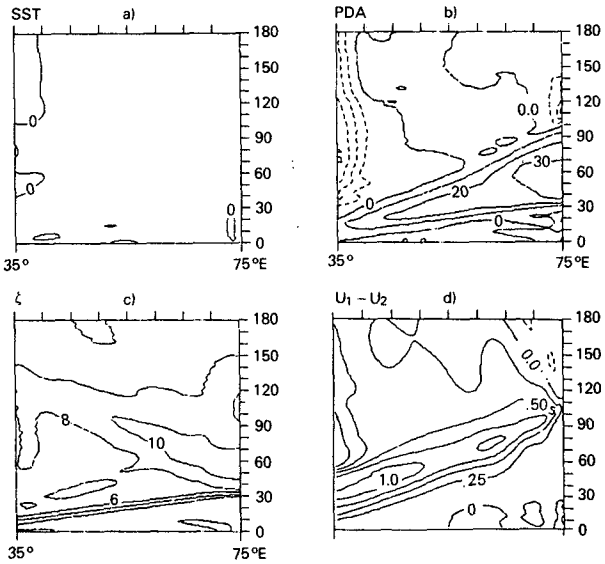

FIG. 5. Equatorial time–longitude sections from the model results with southerly wind forcing. The conditions at the time of onset have been subtracted. Quantities and contour intervals as in Fig. 3.

after K_1 has arrived, it has increased to 26°. The 28° isotherm has been moved from 2.5°S to 3.75°. The arrival of K_2 lifts the 15° isotherm and pushes down the 28° water. 100 days after onset of the perturbing winds, the SST at 5°S has risen to 27.7° and the 28° isotherm moved to 4.5°S.

Together, the two Kelvin waves have caused a 2–3°C warming in coastal SST south of the equator, and they have done so without any detectable SST signal along the equator. The first response in SST is this eastern coastal warming some 40 days after the onset of the wind anomaly.

The Kelvin waves can be seen in heat budgets over small regions of the eastern tropics. Because the mixed layer is free to change its mass, we have evaluated the budgets for both total heat and for the temperature term alone. Fig. 9a shows the budget for the total heat in the mixed layer from 3° to 6°S and within 2° of the coast. The heat balance is between entrainment of cold water (w_eT_e), horizontal advection of heat $\nabla\cdot(uhT)$, surface heating (Q), and vertical diffusion (D). At the end of the initial spin-up the heat is being maintained largely through advective processes, with cold water entering at the base of the layer and leaving the region horizontally. Little influence is seen due to the surface heating. The arrivals of the first and second Kelvin waves are evident in the large change in both horizontal and vertical advection terms.

The temperature balance is somewhat different. Fig. 9b shows the balances for the evolution of $h_1\partial T/\partial t$: entrainment cooling $[w_e(T_e - T_1)]$, zonal advection $(u\partial T/\partial x)$, meridional advection $(v\partial T/\partial y)$, surface

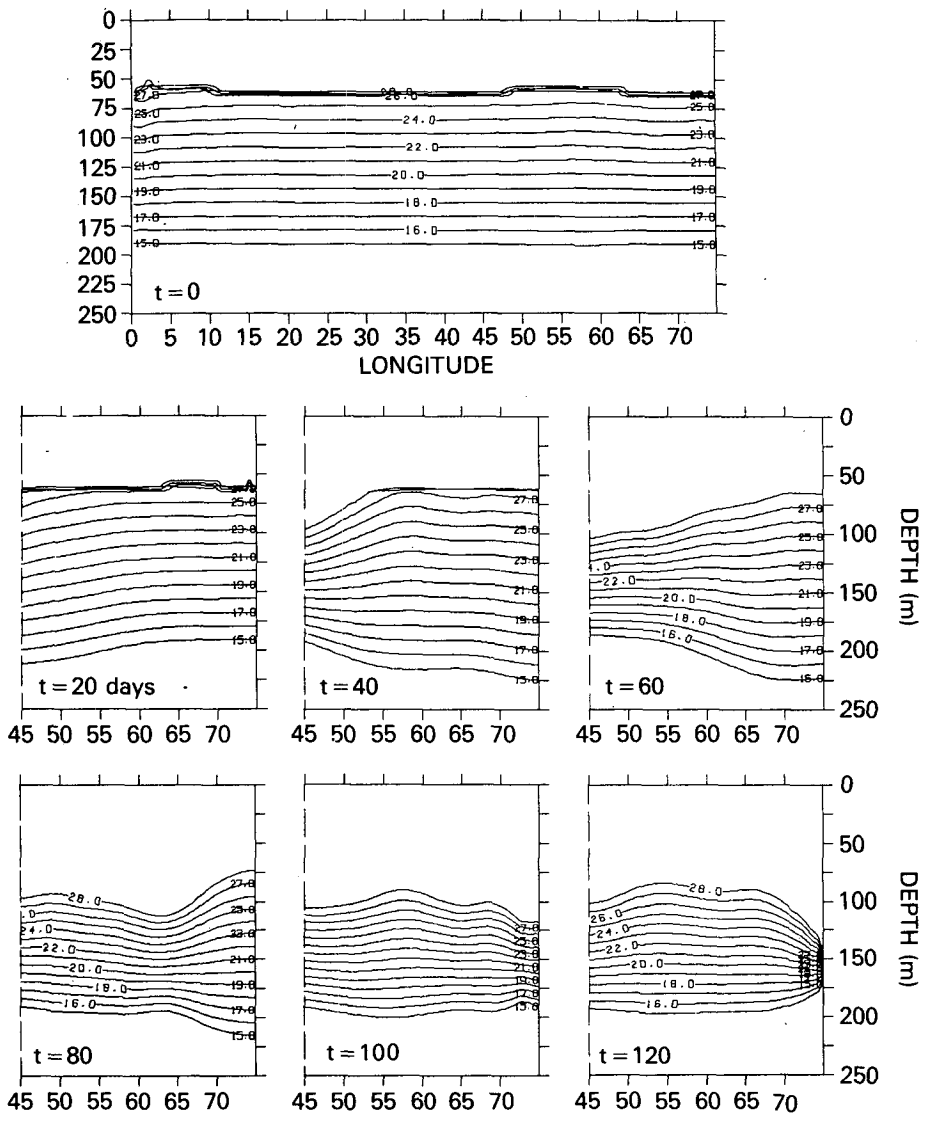

FIG. 6. As in Fig. 4, but for equatorial temperature sections from the southerly mean wind case.

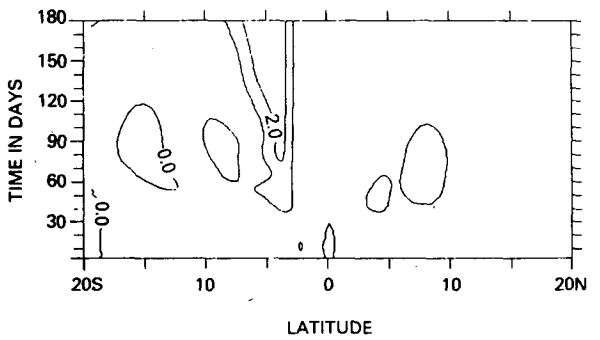

FIG. 7. Latitude–time section behavior of SST near the eastern wall, southerly mean wind forcing. The change in SST is shown after the imposition of the westerly perturbation.

heating (Q), and vertical diffusion (D). The SST is being increased by surface heating as it is being advected horizontally Entrainment sets its initial temperature and so does not appear as a strong factor.

c. *Mean Easterly wind*

The results with mean southerly wind approximate the conditions found in the extreme eastern Atlantic and Pacific Oceans, but the mean state has no equatorial upwelling, undercurrent, nor temperature gradient along the equator. Including these characteristics might be expected to alter the character of the wave responses along the equator.

In this case uniform easterly winds of 0.5 dyn cm^{-2}

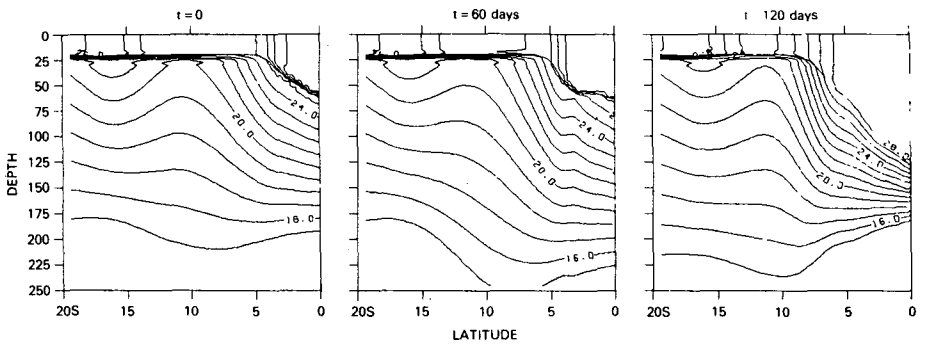

FIG. 8. Temperature sections along the eastern wall south of the equator, southerly mean winds. The panels are separated by 60 days, from the onset of the perturbation.

are imposed over the domain and the model was spun-up for 360 days, before the westerly perturbation was introduced. The initial state shows equatorial upwelling, with cold SST along the equator; Fig. 10 gives the fields of SST, mixed layer depth and velocities in the surface and second layer at the end of the spin-up. A zonal temperature gradient of ~0.2°C per degree of longitude is present, except in the west. The undercurrent is steady and strong, averaging 1.3 m s^{-1}.

To illustrate the effects of the westerly anomaly, we present differences between this run and a control run made by extending the mean forcing without perturbation. Fig. 11 shows the behavior of these differences in longitude-time plots along the equator. The SST now shows a strong warming all along the equator; the warming starts in the *west* and propagates east at the first mode speed (K_1 is seen best in Fig. 11b, the pycnocline depth). At first it appears that the warming stops with the arrival of the second mode, but closer examination of the solutions indicates that the cessation of warming occurs at a given place when $\nabla T = 0$, as the 28°C water arrives. Fig. 12 gives the longitude–time section of SST for the perturbed run, not the differences, and confirms that the cessation of warming and the arrival of water with $\partial T/\partial x = 0$ coincide.

The K_1 propagates into the coast quite linearly, (Fig. 11b) with a signature similar to those in the two previous cases. However, the shear mode behaves quite differently. From the plot of zonal shear (Fig. 11d), the K_2 wave can only be followed to 15–20° east of the forcing region. A drop in speed seems to begin at day 400 near 45–50°E, and propagates to

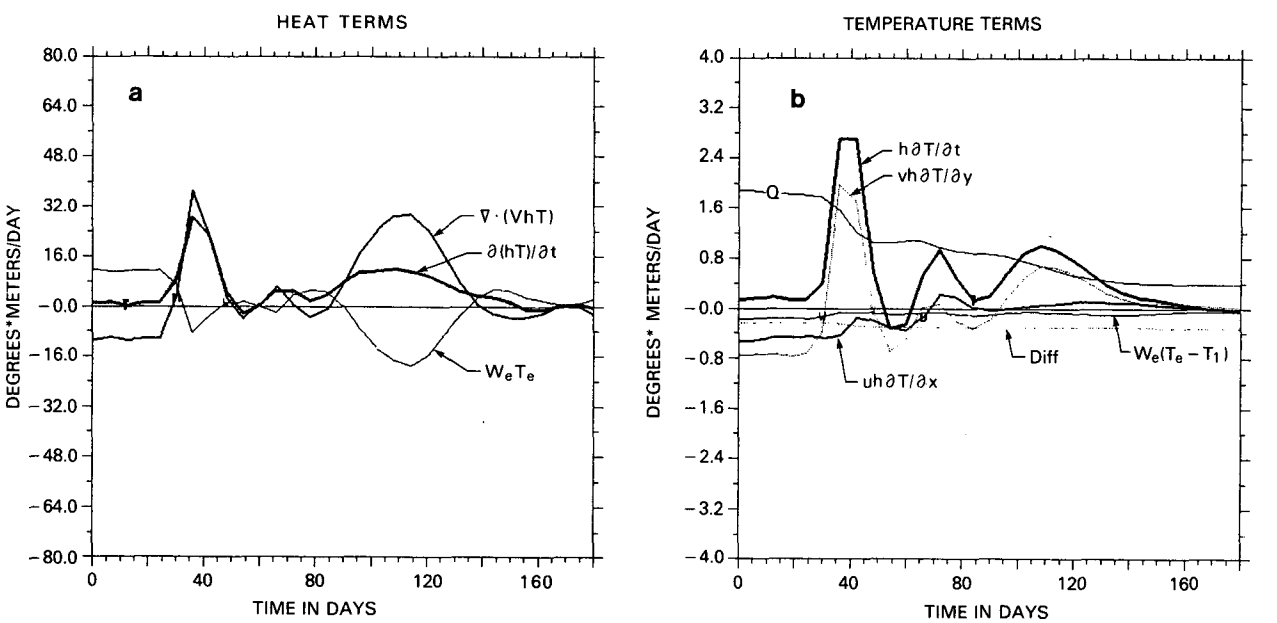

FIG. 9. Heat and temperature budgets over the region 2–6°S, 73–75°E. a) Heat balances: $(hT) = -\nabla(VhT) + w_eT_e + Q - D$. ($Q$ and D are small and omitted from the plot). b) Temperature balances $hT = -hu\partial T/\partial x - hv\partial T/\partial y + w_e(T_e - T_1) + Q - D$. Units are m °C day^{-1}.

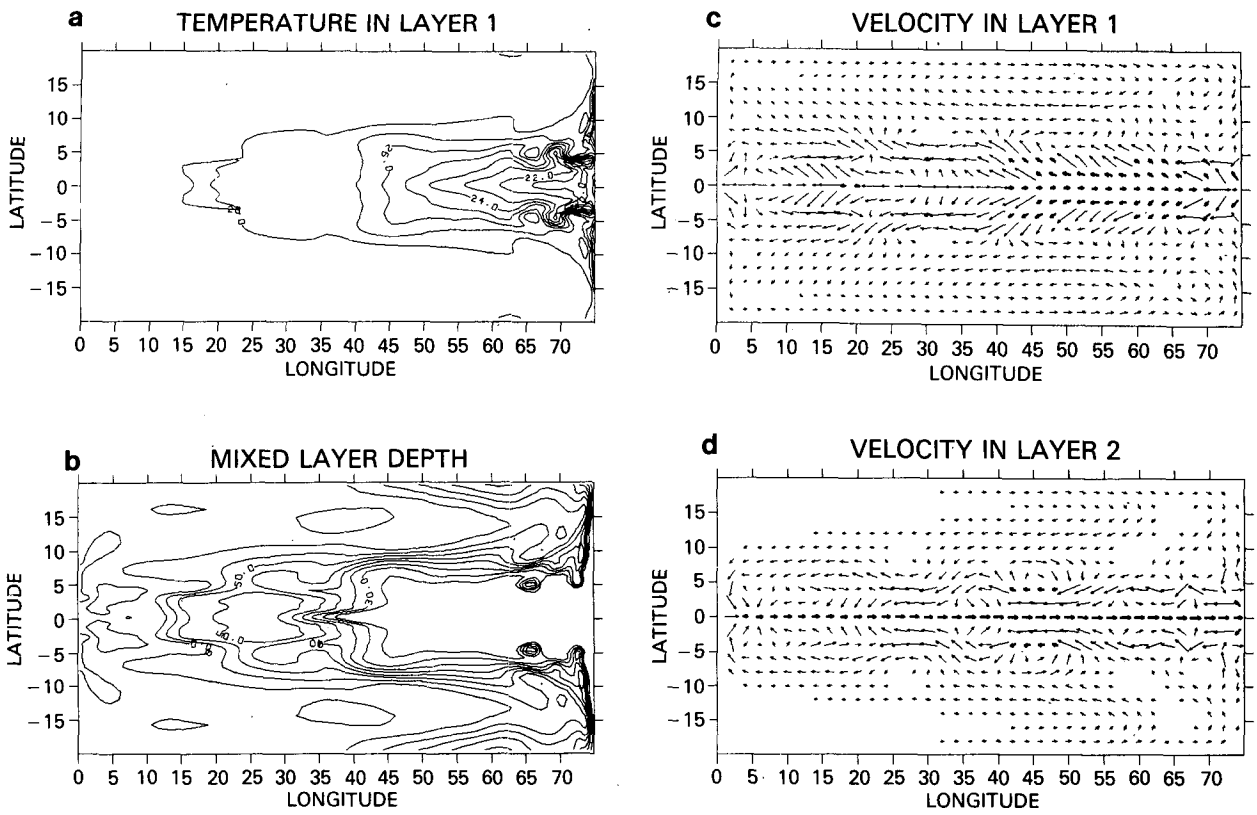

FIG. 10. Initial conditions for mean easterly winds. a) SST, contour interval 1°C, b) mixed layer depth, contour interval 5 m, c) surface velocity and d) undercurrent velocity. The barbs are proportional to the speed, single weight barbs have $0.02 < |V| < 0.40$ m s^{-1}, double weight barbs have $|V| > 0.40$ m s^{-1}.

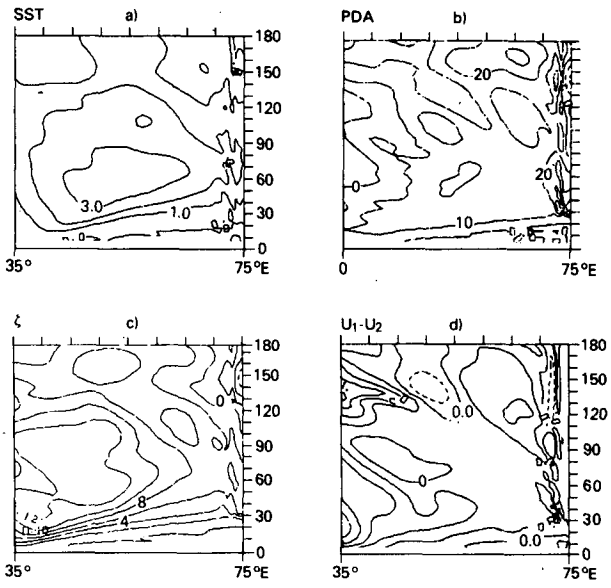

FIG. 11. Equatorial longitude–time sections of the anomaly fields with mean easterly winds, westerly perturbation imposed in western half basin at day 0. Quantities and contour intervals as in Fig. 3 and 5.

the west at a speed appropriate for a Rossby wave. This is not an artifact of the initial spin-up; we ran a second perturbation study, beginning the perturbation after 540 days of spin-up. As ringing waves from the initial spin-up will have a different phase, if they remain at all, we can see if they account for

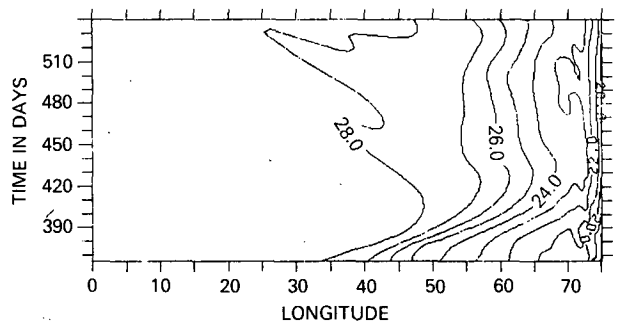

FIG. 12. Equatorial longitude–time section of SST with mean easterly winds, westerly perturbation. The anomaly seen in Fig. 11a stops growing when the SST achieves 28°C. Time is given from the start of the run—the wind perturbation is applied at day 360.

the pattern seen in Fig. 11d. In this repetition, the essential features of Fig. 11 were clearly repeated.

The behavior of the depth of the pycnocline also shows an absence of the shear mode wave. Recall that in the no-mean wind case (Fig. 3b) the shear-mode Kelvin wave draws the pycnocline back up as it passes. Here, there is almost no restoration of the pycnocline once the first mode has deepened it.

The destruction of the K_2 wave can be effected by the mean upwelling associated with the easterly wind stress. The shear mode wave has an eastward flow in the shallow mixed layer and westward flow below. Vertical circulation lifts the westward momentum to the surface and transports the eastward momentum poleward. Thus the structure along the equator changes from a shear mode toward a more depth-uniform flow to the west. This results in a transfer of energy from the second to first model mode. The deposition of eastward momentum at higher latitudes gives rise to a meridional profile in the shear mode that more closely resembles a Rossby than Kelvin wave structure, which apparently propagates off to the west.

The vertical advective change in the mixed layer velocity is the model's means for treating the surfacing of the mixed layer. The momentum placed in the mixed layer has been swept up to the surface and several degrees poleward. The time that this takes to remove all the eastward momentum from the mixed layer is h_1/w, where h_1 is the initial depth, and w is the mean vertical velocity through the mixed layer. Approximating h_1 as 30 m and w as 1 m day^{-1}, the residence time is 30 days. During this time, the shear-mode Kelvin wave can only propagate some 15° to the east. This is consistent with the findings presented in Fig. 11. (Compare Fig. 11d with 3d and 5d).

As noted above, when the solution to (13) yields a value for h_1 that is less than the minimum depth, we impose $h_1 = h_{\min}$. The difference in numerical treatment could lead to a partial computation reflection of wave energy. In this case however, the incident K_2 wave has a downwelling signal at the base of the mixed layer. The wave physics is not affected by the fact $h_1 = h_{\min}$ when the wave arrives. The fact that h_1 stays at $h_{\min}$ despite the downwelling Kelvin wave simply reflects the fact that there is strong large-scale upwelling from the mean meridional circulation.

Along the eastern wall, the appearance of K_1 and the absence of K_2 are clear. Fig. 13 gives the latitude-depth sections of temperature along the eastern wall at 60 day intervals from the onset of the perturbation. At 60 days, the first mode wave has arrived, but K_2 is not yet expected. Deepening of the 15°C isotherm has taken place, together with deepening of all the isotherms in the second layer—a straightforward first mode wave response. At 120 days, the shear mode would have appeared in either of the two previous cases. But here, the response is strikingly unchanged from day 60. There is no second-mode Kelvin wave incident on the eastern coast from a forcing only 37.5° to the west.

The entire SST response in this case is due to the propagation of the first mode Kelvin wave. The advection of temperature along the equator by the eastward flow warms the SST by a sloshing of water associated with the K_1 front. In this case the mean state has very much stronger mean zonal temperature gradients than observed in the Pacific. This exaggerates the effect of a given acceleration in u_1 on dt_1/dt, relative to oceanic conditions. A simple re-scaling of dT/dx to central equatorial Pacific conditions suggests an advective warming of 0.5°C or less for a comparable zonal velocity perturbation.

4. Discussion

We have seen from Section 3 that the equatorial wave response in our model system to a patch of anomalous westerly stress differs in a number of important ways from simple linear model predictions. In particular, we have shown that the changes in SST induced by the passage of the first and second Kelvin-wave fronts (K_1 and K_2) are very strongly a function of the state of the ocean through which they propa-

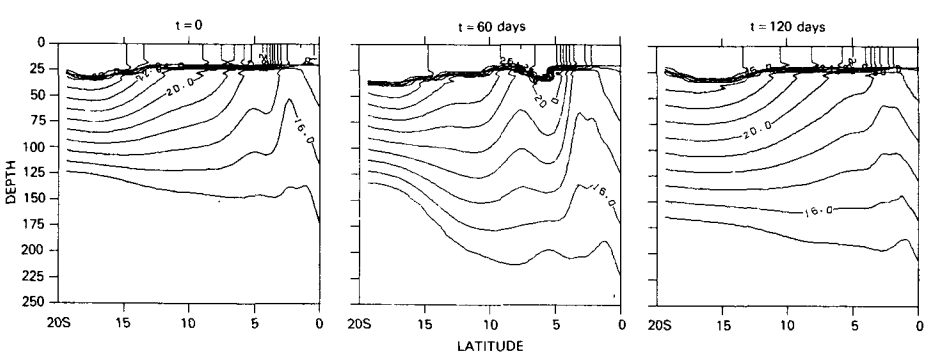

FIG. 13. As in Fig. 8, but for temperature sections along the eastern wall south of the equator, easterly mean winds.

gate, which itself depends upon the winds and heating that have been in effect before the anomaly begins. Generally speaking, SST changes and pycnocline depth changes are not well correlated, so that the assumption of strong correlation that is made in reduced gravity models is not supported by these experiments. Another model result of interest concerns the difficulty of observing passage of the K_2 front in sea surface height, even though K_1 is generally best observed in this field. In these experiments, the effects of K_2 passage are comparable to those of K_1 for SST and subsurface temperature changes along the eastern coast south of the equator; following its progress across the basin is therefore an important step in connecting the wind anomaly to eastern coastal temperature changes.

In every experiment K_1 propagates across the basin at a speed very close to that predicted by linear theory, based on the mean thermal state of the ocean prior to the wind anomaly. In the cases with no mean easterly wind stress along the equator, K_2 also propagates in accord with linear predictions, although its progress is best followed in the $u_1 - u_2$ field. When there is mean easterly stress, however, the K_2 front only propagates 10 to 15° east of the wind patch before it is destroyed by non-linear advections associated with the mean meridional/vertical circulation at and near the equator.

Sea surface temperature and subsurface temperature changes are caused predominantly by advective effects associated with wave frontal passage rather than interactions between mixed layer processes and wave passage. In particular the large equatorial SST warming caused by K_1 passage in the mean easterly wind case results from the existence of a mean negative zonal SST gradient and the eastward u_1 change associated with the wave front passage; this result is quite similar to that of Philander (1981). This effect is not observed with no mean winds or southerly winds because they do not create zonal SST gradients. Also the eastern SST warming observed in the mean southerly wind case results from prior establishment of a mean meridional SST gradient near the coast and the meridional acceleration caused by the Kelvin waves as they propagate down the coast. Temperature changes stop when either the large scale temperature gradient is eliminated or the wave-induced current changes dissappear.

One of the objectives of this idealized study was to gain insight into the role(s) that Kelvin waves, forced by wind changes well west of the eastern coastal boundary, might play in the initiation and continuation of warming events like El Niño. Our results suggest several interesting things: 1) Kelvin waves can cause temperature changes near the east coast comparable to those found at the onset of El Niño events, but the warming can only occur if a cold tongue of water already exists. 2) The propagation of the shear-mode Kelvin wave from its generation region to the east coast depends upon sufficiently weak easterlies along the equator in the region of propagation so that the wave front is not destroyed by the mean circulation before it gets to the coast. 3) Passage of the first-mode Kelvin wave front should be observable in SST changes when there is a mean zonal SST gradient along the equator (scaling our result to near central Pacific conditions from February through May suggests $\Delta SST \sim 0.5°C$ for a wave forced by a 0.5 dyn cm^{-2} anomaly over 20° of longitude). 4) It is possible for the strong SST response to occur first in the eastern part of the basin. Even though the Kelvin wave energy is propagating from the forcing region in the west to the east, the change in SST along the way can be unobservable given the accuracy and resolution offered by present SST data.

These model experiments do not give the broad, strong warming that appears to propagate westward after the first SST signal at the coast during El Niño events. Rather than introduce the complications associated with variable air temperatures, the effect of clouds, etc., this case was run to shed light on the mechanics of the Kelvin wave and the initial SST behavior. We have carried out other experiments on the role of different models of air–sea exchange of heat which greatly increase the areal extent of the cold tongue and give more El Niño-like warming; they will be reported in a companion paper (Schopf, 1983). However, the onset behavior and mechanisms reported here concerning the equatorial and coastal behavior of SST, sea level, pycnocline depth and currents are largely unaffected in these later experiments.

The mixed-layer equations used in this model are the same as those employed in Schopf and Cane (1983), in which important, subtle interactions occurred between the ocean dynamics and the mixed-layer physics. In the spin-up to steady states, fronts were produced and the evolution of the flow substantially altered by these interactions. In contrast, the perturbation results here display no similar interactions. The only feature of the mixed layer that matters here is the difference between entrainment (which cools the SST) and detrainment (which leaves SST unchanged).

There is an important feature of these results which pertains to the study of ocean sea level, SST and deep isotherm displacement records. The most linear and reliable measure of the model's dynamic response is the surface height field (or depth-integrated temperature anomaly). This field responds primarily to the gravest mode in the model (roughly the second baroclinic mode in the ocean), and this mode appears to be quite linear in its perturbation response. The depth of the 15 or 20°C isotherm is much more complex and sensitive to non-linearities, sometimes showing

response in both modes, sometimes not. The pinching action of the shear mode acts here in a fashion that is distributed over the second layer. The susceptibility of the higher mode to vertical non-linear effects, and the inherently shorter length scales associated with its response makes it difficult to predict or analyze response in such fields. The SST response is even more unpredictable. Changes in SST are sensitive to the pre-conditioning of the field before the perturbations are introduced, and so predictions of SST must depend on an adequate description of the past and present thermodynamic balances. Also, the effects of non-linearities on the K_2 shear mode have significant impact on SST evolution in this model study, which makes reliable inferences from extensions of linear theory difficult.

Busalacchi and O'Brien (1981) have compared their reduced gravity model results with sea-level records from the Galapagos. They claim relatively good agreement with strong anomalies (although their results appear to have significantly more high frequency energy than the observations). Correlations between SST and sea-level, however, are not as strong and lagged by some months. The above results suggest why this might be the case. The surface height response due to one mode that is relatively linear in its character should be relatively simple to reproduce. On the other hand, SST changes are fundamentally non-linear and can result from both modes. Thus the correlation with SST records should be weaker. That portion of the SST response which is due to the first mode should be relatively in phase with the sea level changes, but the second mode response will come later. The lag will change as the forcing region for the Kelvin waves varies, since the modes travel at different speeds. Other differences can operate as well. The SST does not change abruptly with the arrival of K_1 or K_2, but merely begins its change at these points. The evolution of the SST is gradual, and it is difficult to sort out the arrival of either of the two modes in the temperature records alone. The use of monthly mean SST data makes it difficult to establish connections between warming and the arrival of particular waves.

It should be pointed out that the two modes used here are approximations of higher linear internal gravity modes. The gravest mode here represents uniform flow down to about 200 m. With conditions as observed in the equatorial Atlantic and Pacific oceans, this mode best approximates the second baroclinic mode, with its first reversal in flow at or below 200 m, and the similarity between the present easterly wind study and Philander's (1981) result reflects this parallel. Philander and Pacanowski (1980) argue that this mode is perhaps the most relevant for the equatorial Pacific. The second mode in the present model is an approximation for a shear mode between the mixed layer and the waters beneath. It has no direct equivalent in the baroclinic set, but represents a collection of the higher modes with such a shear property.

Questions can be raised about the treatment of the surface heat flux in this model. We have chosen what has become a traditional treatment of surface heat flux (Haney, 1971) with the further simplification that the air temperature is uniform at 29°C. We understand that these assumptions are not optimal for studying the flux induced changes in SST, but the heating tendency observed from dynamic processes in these model studies exist independently of particular choices of surface heat-flux parameterizations. In a subsequent study (Schopf, 1983) we investigate further the changes introduced by altering this parameterization. Although the changes in air-sea flux parameterizations do alter aspects of the SST change, the dynamical tendencies discussed here are indeed not affected.

The present study has revealed some features of the thermo- and hydro-dynamic response of the ocean to variable winds, but many issues remain unresolved. In particular it seems important to investigate further whether mixed layer physical processes are indeed relatively unimportant in these situations and whether the reflected Rossby waves can be important under different model assumptions. Clearly the factors which establish the mean state of the Pacific prior to El Niño events also must be better understood. The mean states used here are rather idealized, and the sensitivity of the perturbation results to them indicates that further work is necessary before a full understanding of the role of Kelvin waves in El Niño is possible. We have shown that Kelvin-wave fronts can produce an El Niño-like initial SST response in the east, but understanding the link between the initial Kelvin wave induced coastal warming and the broad, strong anomalous SST seen in Rasmusson and Carpenter (1982) requires more study.

Acknowledgments. We wish to thank Tom Kuscera and Ken Young for programming assistance. PSS was supported in this work by National Aeronautics and Space Administration (NASA) RTOP 161-20-21. DEH was supported by National Science Foundation Grant NSF OCE 80-24117 and NASA Grant NGT 22-009-900 to the Massachusetts Institute of Technology.

REFERENCES

Busalacchi, A. J., and J. J. O'Brien, 1981: Interannual variability of the equatorial Pacific in the 1960's. *J. Geophys. Res.*, **86**, 10901–10907.

Cane, M. A., and E. S. Sarachik, 1976: Forced baroclinic ocean motions. I: The linear equatorial unbounded case. *J. Mar. Res.*, **34**, 629–665.

——, and ——, 1977: Forced baroclinic ocean motions. II: The linear equatorial bounded case. *J. Mar. Res.*, **35,** 395–432.

Haney, R. L., 1971: Surface thermal boundary condition for ocean circulation models. *J. Phys. Oceanogr.*, **1,** 241–248.

Hurlburt, H. E., J. C. Kindle and J. J. O'Brien, 1976: A numerical simulation of the onset of El Niño. *J. Phys. Oceanogr.*, **6,** 621–631.

Kraus, E. B., and J. S. Turner, 1967: A one-dimensional model of the seasonal thermocline. II: The general theory and its consequences. *Tellus*, **19,** 98–109.

Matsuno, T., 1966: Quasi-geostrophic motions in the equatorial area. *J. Meteor. Soc. Japan*, **44,** 25–43.

McCreary, J. P., Jr., 1976: Eastern tropical response to changing wind systems: with application to El Niño. *J. Phys. Oceanogr.*, **6,** 632–645.

——, 1981: A linear stratified ocean model of the equatorial undercurrent. *Phil. Trans. Roy. Soc.*, **A298,** 603–625.

Moore, D. W., and S. G. H. Philander, 1977: Modeling of the tropical oceanic circulation. *The Sea*, Vol. 6, E. Goldberg *et al.*, Eds., Wiley-Interscience. 319–361.

Niiler, P. P., and E. B. Kraus, 1977: One dimensional models of the upper ocean. *Modeling and Prediction of the Upper Layers of the Ocean*, E. B. Kraus, Ed., Pergamon Press. 143–172.

Philander, S. G. H., 1981: The response of equatorial oceans to a relaxation of the trade winds. *J. Phys. Oceanogr.*, **11,** 176–189.

——, and R. Pacanowski, 1980: The generation of equatorial currents. *J. Geophys. Res.*, **85,** 1123–1136.

Rasmusson, E. M., and T. H. Carpenter, 1982: Variations in tropical sea surface temperature and surface wind fields associated with the Southern Oscillation/El Niño. *Mon. Wea. Rev.*, **110,** 354–384.

Schopf, P. S., 1983: On equatorial Kelvin waves and El Niño: II. Effects of Air-Sea Thermal Coupling. *J. Phys. Oceanogr.* (in press).

——, and M. A. Cane, 1983: On equatorial dynamics, mixed layer physics and sea surface temperature. *J. Phys. Oceanogr.*, **13,** 917–935.